Received 21 April 2015; revised 6 November 2015 and 19 November 2015; accepted 23 November 2015.
Date of publication 25 November 2015; date of current version 29 December 2015.

*Digital Object Identifier 10.1109/JXCDC.2015.2504049*

# Coupled-Oscillator Associative Memory Array Operation for Pattern Recognition

**DMITRI E. NIKONOV[1] (Senior Member, IEEE), GYORGY CSABA[2], WOLFGANG POROD[2] (Fellow, IEEE), TADASHI SHIBATA[3] (Member, IEEE), DANNY VOILS[4], DAN HAMMERSTROM[5] (Life Fellow, IEEE), IAN A. YOUNG[1] (Fellow, IEEE), AND GEORGE I. BOURIANOFF[1] (Member, IEEE)**

[1]Components Research, Intel Corporation, Hillsboro, OR 97124 USA
[2]Center for Nano Science and Technology, University of Notre Dame, Notre Dame, IN 46556 USA
[3]Emeritus of Electrical Engineering, The University of Tokyo, Tokyo 113-8656, Japan
[4]Department of Electrical Engineering, Portland State University, Portland, OR 97207-0751 USA
[5]Defense Advanced Research Projects Agency, Arlington, VA 22203-2114 USA

CORRESPONDING AUTHOR: D. E. NIKONOV (dmitri.e.nikonov@intel.com)

This work was supported by Intel Labs of Intel Corp. within the NBAD Program.

**ABSTRACT** The operation of an array of coupled oscillators underlying the associative memory function is demonstrated for various interconnection topologies (cross-connect and star-coupled). Three types of nonlinear oscillators (Andronov–Hopf, phase-locked loop, and spin torque) and their synchronization behavior are compared. Frequency-shift keying scheme of encoding input and memorized data is introduced. The speed of synchronization of oscillators and the evolution of the degree of match are studied as a function of device parameters.

**INDEX TERMS** Array, associative memory, neural networks, non-Boolean computing, oscillator, phase-locked loop (PLL), sparse representation, spin torque.

## I. INTRODUCTION

THE progress of integrated circuits for digital computing has been an unprecedented success for the past 40 years due to scaling of the number of transistors on chip (Moore's law [1]). Continued scaling is projected for at least another decade [2]. Digital circuits thus handily meet user requirements for the processing of numerical, text, and video information. However, there is a class of problems, traditionally associated with human intelligence, which computers do not handle as successfully. They are, for example, image recognition, speech recognition, contextual search, and detection of spatiotemporal events. Algorithms for their solution based on digital Boolean logic exist, but require excessive computational effort. Various researchers arrived at the idea to explore alternative analog or non-Boolean methods of computing for these problems. A school of thought that aimed to emulate, to various degrees, the operation of neurons emerged. It resulted in vigorous growth of the fields of neural networks [3] and neuromorphic computing [4]. Various architectures for non-Boolean computing exist. Artificial neural networks [5] are the cascaded devices with typically high fan-in and fan-out. Cellular neural networks [6] are typically rectangular arrays of nodes, each connected to nearest neighbors. LEGION networks [7] combine coupling between nearest neighbor oscillators with a common inhibiting node. In contrast to the above approaches, we are dealing in this paper with networks of oscillators, which we call coupled-oscillator associative memory array (COAMA). In such a network, all oscillators are coupled to each other, possibly through a common node (the averager). The memorized and test patterns are encoded in the parameters of oscillators. Under proper operation, if a test pattern is close to one of the memorized patterns, the phases of oscillators synchronize, which we interpret as recognition. However, if the phases of oscillators do not synchronize, it is a lack of recognition.

Our work builds on prior research in [8]–[10]. But, in this paper, we are going further. We design realistic schemes of such oscillator arrays using particular nanoscale devices [such as nanotransistors and spin-torque oscillators (STOs)]. Prior work with coupled oscillators used a scheme, in which the patterns are encoded as constants of coupling between

oscillators [phase-shift keying (PSK)]. Correspondingly, two stages—initialization and recognition—were required in PSK. Here, we present for the first time a scheme of frequency-shift keying (FSK), in which the patterns are encoded as the differences of frequencies of oscillators. FSK requires only a single stage of recognition. In addition, we use more realistic mathematical models for simulating oscillators than the popular models. For example, the Kuramoto model [11], [12], which has been widely used to represent arrays of coupled oscillators, contains only phases of oscillators. In contrast, all our models involve both amplitudes and phases of oscillators. This holds true for our phase-locked loop (PLL) model being more rigorous than that in [13].

For arrays of STOs [14], we extend our treatment from the macrospin model (describing the magnetization of a nanomagnet by a single vector) to a micromagnetic simulation (capturing the coordinate dependence of magnetization). Thus, the STOs are described with the most physically based model than the other two types of oscillators. For realizing dynamic, non-Boolean computing systems, we explore an avenue where basic device components are not trying to imitate a CMOS switch or circuit dynamics, but where the individual device components itself are complex dynamical systems. The benefits of oscillatory non-Boolean systems could potentially be better exploited using such devices. As an example, we study the spin-torque oscillators described in STOs that are sub-100-nm-scale devices, acting as compact microwave oscillators [15]–[20]. The self-sustaining oscillations are generated by the flow of spin-polarized currents (spin torque) into a thin magnetic layer, and the magnetization oscillations can be detected by the resistance change in the same current path [21]. The magnetic oscillations may create propagating spin waves [22], [23], which provide a nonelectrical interaction mechanism between STOs [24]. The physics underlying STO operation is, in principle, well understood and one can use standard micromagnetic simulation codes [25] to model magnetization dynamics. However, due to the strong nonlinearity of magnetization dynamics [26], the large variety of possible oscillation [27] and spin-wave modes, and the heavy computational workload of a full micromagnetic simulation, one has to use a hierarchical set of approximate modeling tools to understand the behavior of STO networks. This paper presents such modeling hierarchy.

The coupling constants between oscillators correspond to the Hopfield network algorithm. We compare it with other associative memory algorithms (Palm and Furber/Willshaw) in the Supplementary Material. We analyze the accuracy of recognition of these algorithms, first using random data patterns and then feature patterns extracted from real-life images.

## II. ASSOCIATIVE MEMORY AND OSCILLATOR ARRAYS

The role of an associative memory is to compare a vector of a test pattern with the set of $m$ vectors of memorized patterns and to find one (or several) closest according to some metric defined for these vectors

$$\text{test} = \xi_0, \quad \text{memorized} = \xi_1, \xi_2, \xi_3 \ldots \tag{1}$$

where the vectors can be of any length $n$, binary, or grayscale. A simple example of patterns in Fig. 1 will be used for an illustration here. We apply an array of coupled oscillators to the task of recognition and seek a design where the synchronization of oscillators would correspond to a match. We start with describing the evolution of an array of Andronov–Hopf oscillators [28] (similar to van der Pol oscillators) by

$$\frac{dz_i}{dt} = (\rho_i + i\omega_i)z_i - z_i|z_i|^2 + \varepsilon \sum_{j=1}^{n} C_{ij} z_j \tag{2}$$

where $z = x + iy$ is the complex amplitude of an oscillator, $\rho_i$ is a parameter determining the limiting cycle amplitude, $\varepsilon$ is the strength of coupling between oscillators, and the subscripts $i$ and $j$ denote the oscillators within the array and, correspondingly, the elements in the vectors. This model closely follows those of other efforts [8]–[10]. In these examples, we will use $\rho_i = 0.03$ and $\varepsilon = 0.01$.

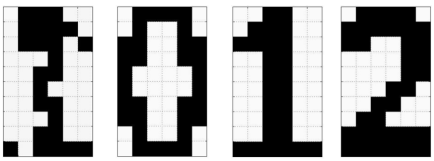

**FIGURE 1. Example 1 × 60 patterns. Left-most pattern is the test one, and the rest of the patterns are memorized. The 1-looking test pattern is the closest to the middle memorized pattern.**

We consider two methods of encoding of patterns into oscillators: 1) FSK (introduced for the first time in this paper) and 2) PSK. The mathematics of PSK has been given in [8]–[10]. In FSK, the patterns are encoded as the frequency shifts of the oscillators. Each associative array (one per memorized pattern) is used to compare the test vector with index 0 with one memorized vector with index $m$, by shifting the frequency of each oscillator labeled by $i$ from the center frequency $\omega_0$, as shown in Fig. 2

$$\omega_i = \omega_0 + \Delta\omega(\xi_{0,i} - \xi_{m,i}). \tag{3}$$

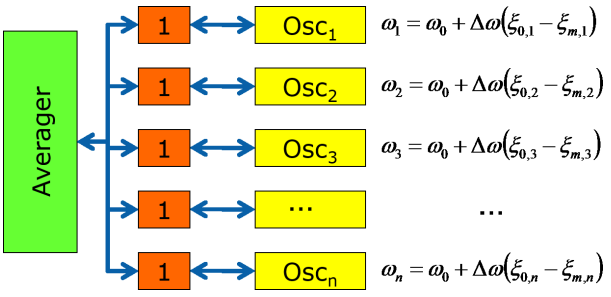


**FIGURE 2. Block diagram of an associative array in the FSK method. Signals are passed in both directions through links.**

The coupling constants are set to a fixed value, e.g., $C_{ij} = 1$. In other words, the memorized and test patterns are encoded not as coupling elements, but as states of the circuits controlling the frequencies of oscillators. The physical implementation of such circuits is dictated by the nature of oscillators. The degree of match (DOM) between the patterns is defined (under the name of mean field activity) in [8] as the amplitude of the following expression to measure the alignment of phases of the oscillators. It is alternatively called Kuramoto synchronization index

$$d_m = \frac{1}{n}\sum_{j=1}^{n} z_j. \tag{4}$$

It corresponds to the amplitude of the signal at the averager.

Intuitively, the reason that the patterns are matched is the dependence of synchronization on the frequencies of oscillators. If the test and the memorized patterns are close, the shifts of oscillator frequencies from the center one will be small. It has been discovered long ago [29] that the coupled oscillators synchronize if their frequencies are different by less than a certain range dictated by the strength of coupling. Conversely, if the test and the memorized are significantly different, many oscillators will be significantly detuned from the center frequency. In this case, the array of oscillators would fail to synchronize to a single frequency. If the array synchronizes, the outputs of oscillators add in phase and the DOM is large. If the array does not synchronize, the phases of oscillators drift relative to each other and their outputs add to an oscillating function that is close to zero amplitude. Note that adding a constant to all elements of a vector does not change the conditions for synchronization. Thus, a uniformly darker or brighter grayscale pattern would still be recognized as a match in FSK.

Pattern matching is obtained differently in the case of PSK. The following mapping of patterns on physical values is used: the logical bit value $b$ takes the values of 1 or 0, and corresponds to the phase of an oscillator $\phi = \pi b$, and the pattern values are $\xi = \cos\phi$, i.e., 1 to $-1$ corresponding, respectively, to white and black. The center frequencies of all oscillators are set to a fixed value $\omega_0$. The coupling constants (weights) are set by the product of pattern values. For the first stage, initialization (Fig. 3), the pattern values are determined by the test vector $\xi_0$, such that

$$C_{ij}(\text{init}) = \xi_{0,i}\xi_{0,j}. \tag{5}$$

The purpose of the initialization stage is to impose the phase differences corresponding to the test pattern on the array of oscillators starting from random initial conditions. For the second stage, recognition, the coupling constants (weights) are switched to the ones determined by all $m$ of the memorized vectors according to a Hebbian learning rule [8]

$$C_{ij}(\text{recog}) = \frac{1}{m}\sum_{k=1}^{m} \xi_{k,i}\xi_{k,j}. \tag{6}$$

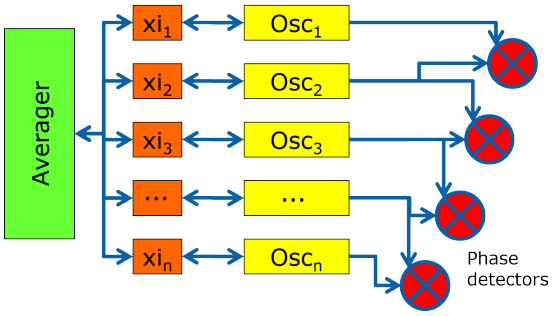


**FIGURE 3. Block diagram of an associative array in the PSK method with star topology in the initialization stage. Signals are passed in both directions through links and multiplied by a factor each time passing an orange box. Phase detectors provide relative phases of neighboring oscillators.**

In other words, all of the memorized patterns participate in the determination of dynamics of oscillators. Experience shows [8] that each pattern corresponds to an attraction basin in the configuration space. The purpose of the recognition stage (Fig. 4) is, for thus prepared oscillators, to transition to the phase differences corresponding to one memorized pattern closest to the test pattern. In both stages, the DOM of the oscillator state to any vector with index $k$ is given by [8] the amplitude of

$$d_k = \frac{1}{n}\sum_{j=1}^{n} \xi_{k,j} z_j. \tag{7}$$

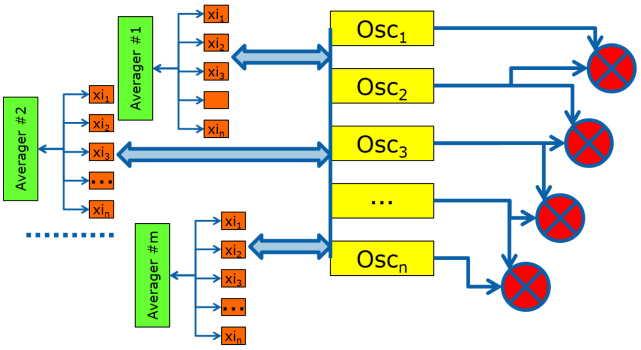


**FIGURE 4. Block diagram of an associative array in the PSK method with star connection topology in the recognition stage. Similar to that of Fig. 3, but the array of oscillators is simultaneously connected to *M* averages.**

The PSK can be implemented with two topologies: 1) star [9], [10] or 2) cross-connect [13]. Both are mathematically equivalent [30] (if one does not consider realistic details of implementations, such as attenuation and delay of signals) and thus would produce identical simulation results. This equivalence can be understood by expressing the coupling term in (2) in terms of memorized or test vectors according to (6) and (7)

$$\varepsilon\sum_{j=1}^{n} C_{ij} z_j = \frac{\varepsilon}{m}\sum_{j=1}^{n}\sum_{k=1}^{m} \xi_{k,i}\xi_{k,j} z_j = \frac{n\varepsilon}{m}\sum_{k=1}^{m} \xi_{k,i} d_k. \tag{8}$$

In the first form in this equation, these terms are implemented by cross-connect coupling, as shown in Fig. 5. In the second form, it is implemented by first summing the outputs by averagers $d_k$ corresponding to each pattern, and then broadcasting the value of each averager to each oscillator, as shown in Fig. 4. Vector elements $\xi_{k,i}$ should correspond to multipliers in each coupling.

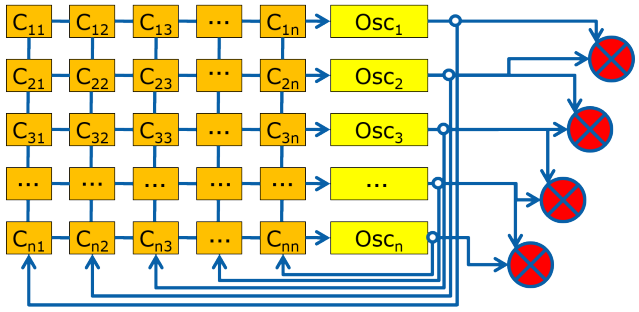


**FIGURE 5. Block diagram of an associative array in the PSK method with cross-connect topology in either the initialization or recognition stages. Signals are passed in one direction in a loop and multiplied by a factor $C_{ij}$ each time passing an orange box. All signals in rows are summed and sent to drive inputs of oscillators. Phase detectors provide relative phases of neighboring oscillators.**

For the initialization stage, the oscillators are connected to one averager (Fig. 3). For the recognition stage, the oscillators need to be disconnected from the averager corresponding to the test pattern and connected to a set of averagers corresponding to the memorized patterns (Fig. 4). For $M$ memorized patterns, one need $M$ averagers. In the cross-connect implementation (Fig. 5), there are no averagers, and the DOM cannot be directly obtained. Thus, one is forced to determine the differences of the phases between neighboring oscillators and compare them with the memorized patterns. This puts this implementation at a disadvantage compared with the star architecture. Its advantage is that for the recognition stage, the scheme is the same and the same number of coupling elements is needed for any number of memorized patterns. In all the above implementations, one can use phase detectors to determine the relative phases of oscillators in order to retrieve the memorized pattern to which the array converged.

## III. FREQUENCY-SHIFT KEYING VERSUS PHASE-SHIFT KEYING SYNCHRONIZATION

The results of simulation of arrays according to (1)–(7) with randomly set initial conditions are shown below. The phase differences of each of the 60 oscillators and the first oscillator are plotted. Time is in units of inverse cyclic central frequency of the oscillators $\omega_0^{-1}$.

First, we consider the FSK example. We see that for a match (Fig. 6), the phases converge to constant values, modulo $2\pi$, from each other. This proves that the oscillators are running at the same frequency and, moreover, are phase locked (synchronized). The DOM reaches a high

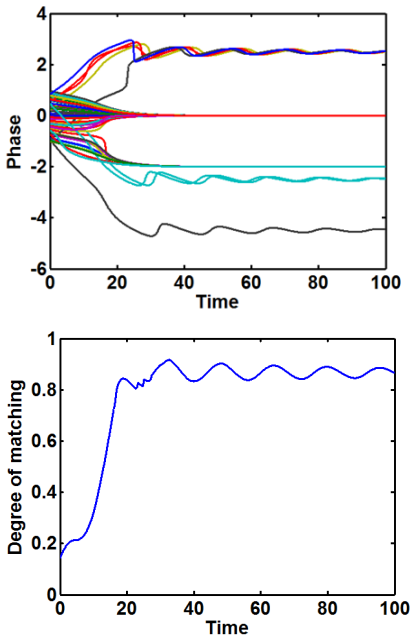


**FIGURE 6. Relative phases of oscillators in units of $\pi$ (top) and the DOM (bottom) versus time for the associative array comparing the test pattern and the 1-looking memorized pattern by FSK.**

value (close to 1) and oscillates weakly around it. Thus, the synchronization is achieved over 6–10 periods of oscillation. Conversely, for the case of bad match (Fig. 7), the phases of most oscillators continue to increase linearly.

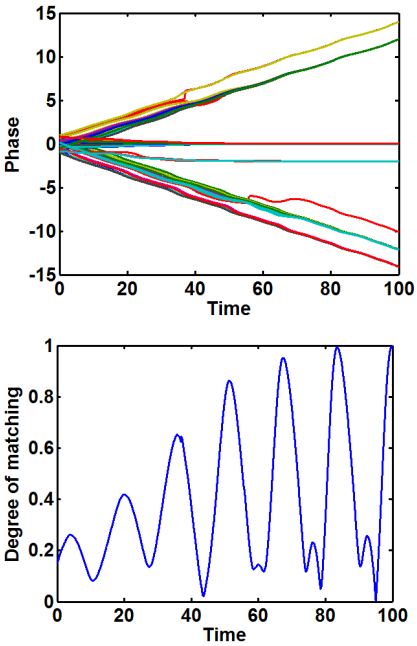


**FIGURE 7. Relative phases of oscillators in units of $\pi$ (top) and the DOM (bottom) versus time for the associative array comparing the test pattern and the 0-looking memorized pattern by FSK.**

This indicates that the synchronization has not occurred for some of the oscillators and the oscillators are running independently with their own frequencies. The DOM oscillates with a large amplitude around a small value. These features of the DOM allow one to build circuits for the determination of a winner-take-all (WTA) or $k$-WTA.

Next, we treat the PSK example. The results of simulations of the evolution of oscillators in their initialization stage are shown in Fig. 8, and for the recognition stage are shown in Fig. 9. They show that the oscillators, starting from random initial amplitude and phase, quickly converge to phases different by $\pi$ or $2\pi$, depending on the sign of coupling constants $C$. The DOM to the test vector reaches 1. Then, in the recognition stage, only a few oscillators switch their phases by $\pi$ in very fast transitions until the DOM to one memorized vector increases to 1, while the DOM to others decreases to 0.

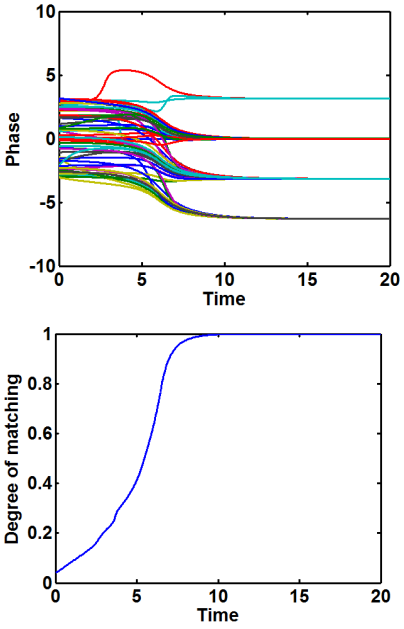


**FIGURE 8. Relative phases of oscillators (top) and the DOM (bottom) versus time for the associative array in PSK initialization stage.**

In PSK, the grayscale patterns are encoded via the phase as $\xi = \cos\phi$. There is an inherent ambiguity of mapping a certain element of the vector to other phase $\phi$ or $-\phi$. Our simulations show that the PSK does not converge to a steady-state solution. We speculate that this is due to multiple possible combinations of angles to which the system can converge.

The overall comparison of the FSK and PSK methods is given in Fig. 10. PSK requires just one oscillator array to find the best matching memorized pattern. FSK calculates the DOM of the test pattern with one of the $m$ memorized patterns. The full associative memory operation required $m$ such arrays in parallel. Additional circuits (such as $k$-WTA) are required to rank the comparisons between each other.

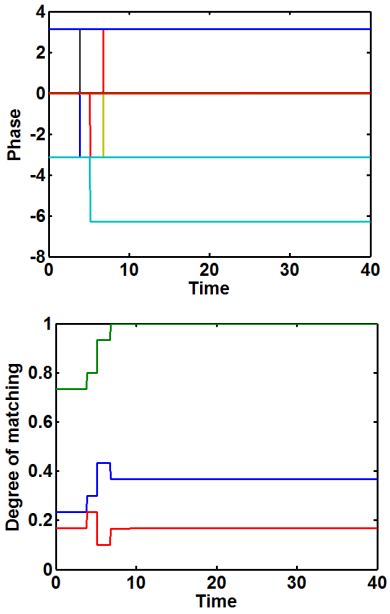


**FIGURE 9. Relative phases of oscillators (top) and the DOM (bottom) versus time for the associative array in PSK recognition stage.**

| Attribute | PSK cross | PSK star | FSK star |
|---|---|---|---|
| Memorized patterns | m | m | 1 * m |
| Averagers | 0 | m | 1 * m |
| Oscillators | n | n | n * m |
| Memory elements | n*n | m*n | 0 |
| Coupling | Real | Binary | Constant |
| Grayscale inputs | Cannot | Cannot | Can |

**FIGURE 10. Table of comparison of the characteristics of PSK and FSK associative arrays. Only local memory elements in the arrays are counted. Possible storage of vectors outside the array is disregarded. *m* arrays in parallel required for FSK.**

The pattern information for FSK can be stored externally to the arrays (with only the difference between input and stored pattern entering the system during evaluation), while the memory elements in the PSK system must be an integral part of the array. The fact that the FSK is capable of handling grayscale inputs, and the absence of variable coupling constants in it, in our opinion, gives crucial advantages to FSK.

## IV. PHASE-LOCKED LOOP SYNCHRONIZATION

Another implementation of oscillators is a PLL with input $v_i$ and output $v_o$, as shown in Fig. 11. Here, we provide a model

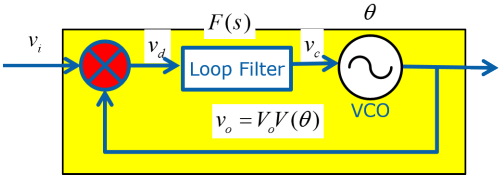


**FIGURE 11. Block diagram of a single PLL, adapted from [13]. It represents one oscillator in the array block diagrams.**

following [31], which includes both phase and voltage amplitudes, more general and rigorous than that in [13] which only includes phase. For the voltage-controlled oscillator (VCO), its phase $\theta$ derivative is modified by the input voltage $v_c$ with the gain $K_0$

$$\frac{d\theta}{dt} = \omega + K_0 v_c \tag{9}$$

where voltage $v_c$ is the output of a loop filter with input $v_d$, described here by a one-pole transfer characteristic with time constant $\tau$

$$\tau \frac{dv_c}{dt} = -v_c + v_d \tag{10}$$

where voltage $v_d$ is coming from a phase detector which can be implemented as an ideal mixer with a factor $A_m$

$$v_d = A_m v_i v_0. \tag{11}$$

We assume that the waveform generated by the oscillator is approximated by a simple harmonic

$$V(\theta) = \cos(\theta). \tag{12}$$

Then, the equations for an array of linearly coupled VCOs, where the sum of outputs of all PLLs is connected to each input

$$\frac{d\theta_i}{dt} = \omega_i + K_0 v_{c,i} \tag{13}$$

$$\tau \frac{dv_{c,i}}{dt} = -v_{c,i} + 2\varepsilon K_d V(\theta_i) \sum_{j=1}^{n} C_{ij} V(\theta_j - \pi/2) \tag{14}$$

where an arbitrary phase delay in the feedback loop is chosen to be $\pi/2$, and the gain of the mixer is

$$K_d = \frac{A_m V_o^2}{2}. \tag{15}$$

The DOM is determined in a manner similar to the above

$$d_k = \frac{1}{n} \left| \sum_{i=1}^{n} \xi_{k,i} \exp(i\theta_i) \right|. \tag{16}$$

The simulation results (Figs. 12 and 13) are qualitatively similar to the case of Andronov–Hopf oscillators. Thus, the synchronization develops in a very similar manner for the oscillators, which are different in the number of variables, the character of nonlinearity, and a form of coupling. Simulations of FSK arrays with PLL (not shown here) are also similar to the results of Section III. This gives us an indication that the very phenomenon of synchronization rather than the nature of the oscillator controls the operation of the associative memory.

## V. SPIN-TORQUE OSCILLATOR SYNCHRONIZATION

STOs are the promising components for oscillatory associative memories. They dissipate very little power (can be driven by milliamps of currents and millivolts of voltage), produce oscillations in the gigahertz range (which is highly compatible with microelectronic circuitry), and enable various interconnection topologies (passive and electrical connections as

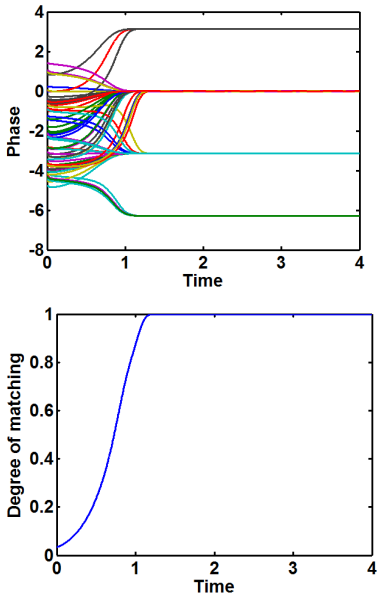


**FIGURE 12.** Relative phases of PLLs (top) and the DOM (bottom) versus time for the associative array in PSK initialization stage.

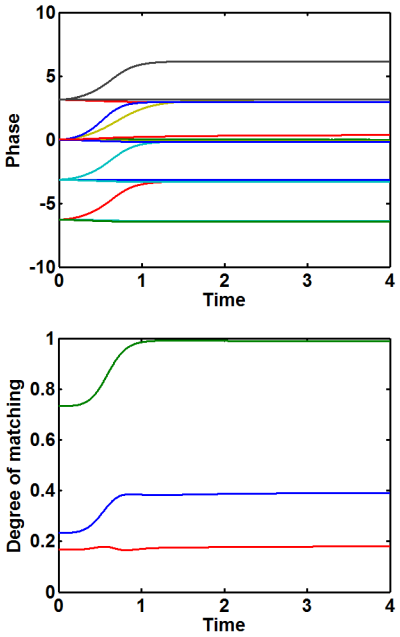


**FIGURE 13.** Relative phases of PLLs (top) and the DOM (bottom) versus time for the associative array in PSK recognition stage.

well as direct spin-wave coupling) [17]. Phase locking of two STO has been demonstrated [24].

The dynamics of STOs is more complicated than that of an idealized oscillator, and to the best of our knowledge, the dynamic equations of the magnetization cannot be reduced to Kuramoto phase oscillators [11] or the previously described Andronov–Hopf oscillators. Our numerical models, however, show that the collective behavior of coupled STOs is very similar to that of the simpler oscillators. In order to demonstrate this: 1) the partial differential equations (PDEs),

micromagnetic equations describing spin-torque driven magnetization dynamics will be written in the form of ordinary differential equations (ODEs) and 2) how phase and frequency locking develops in systems of coupled STOs will be shown.

Numerical solution of the Landau–Lifshitz–Gilbert (LLG) equation is widely used for physics-based simulation studies of the magnetization dynamics in submicrometer-size nanomagnets. In order to model spin-torque effects, the LLG equations are complemented with the Slonczewski antidamping spin-torque term [17]

$$\left.\frac{d\mathbf{M}}{dt}\right|_{\text{prec}} = -\gamma\,(\mathbf{M}\times\mathbf{H}_{\text{eff}}) + \frac{\alpha\gamma}{\mathbf{M}_s}[\mathbf{M}\times(\mathbf{M}\times\mathbf{H}_{\text{eff}})] + \frac{\gamma\beta P_{eff}}{M_s}[\mathbf{M}\times(\mathbf{S}\times\mathbf{M})]$$
$$\beta = \left|\frac{\hbar}{\mu_0 e}\right|\frac{J}{tM_s} \quad P_{eff} = \frac{P\Lambda^2}{\left(\Lambda^2+1\right)+\left(\Lambda^2-1\right)(\mathbf{M}\cdot\mathbf{S})} \tag{17}$$

where $\mathbf{M}$ is the magnetization vector distribution of the free magnetic layer, $\gamma = 2.21\cdot 10^5$ m/(As) is the Landau–Lifshitz gyromagnetic ratio, $e$ is the electron charge, $H_{\text{eff}}$ is the effective magnetic field (which includes contributions from the STO shape, anisotropy, and exchange stiffness), $M_s$ is the saturation magnetization (we used $M_s = 8.6\cdot 10^5$ A/m), $\alpha$ is the damping constant, $J$ is the current density, $\Lambda$ is the spin asymmetry parameter (we used $\Lambda = 1.5$ everywhere), $t = 5$ nm is the thickness of the free layer, and $S$ is a unit vector indicating the spin polarization of the driving current. The vector $S$ is determined by the magnetization direction of a polarizer magnetic layer, but the magnetization of this layer is assumed to be fixed and not simulated. The above parameters are similar to the STOs discussed in [20]. These equations can be applied in two different ways. As written above, they are PDEs, which give the response of a magnetization distribution to an applied external field and current distribution—these are all vector field variables. Micromagnetic solver packages, such as the well-established Object-Oriented Micromagnetic Framework (OOMMF) code [25], are available for the solution, but solving these PDEs is time consuming, and it is difficult to find connections to a Kuramoto-type phase model. For sufficiently small-sized STOs, one can replace the magnetization distribution with a magnetization vector and solve for only ODEs instead of PDEs. This approximation is usually referred as the single-domain or macrospin model. The $M$ and $H$ vector fields are represented by their volume average over the free layer. There is no general rule when such approximation is valid, so the macrospin model should always be carefully validated against the full micromagnetic model.

We performed this comparison for various-sized STOs. For an STO with a $d < 30$-nm-diameter free layer, the macrospin model yields almost identical results to the PDE-based, full micromagnetic description. The frequency–current plot of Fig. 14 gives a side-by-side comparison.

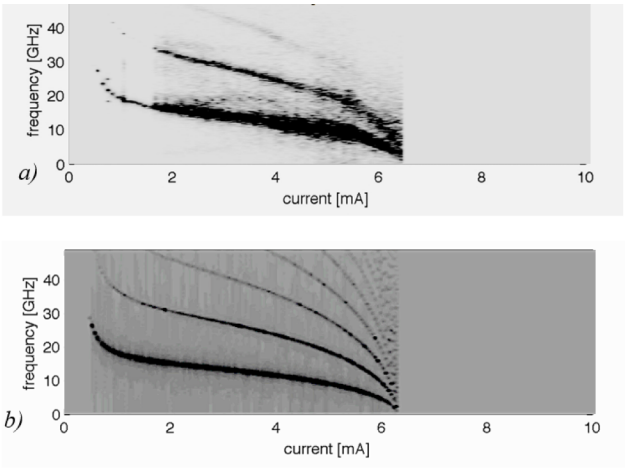


**FIGURE 14. Frequency-current diagram for a 30-nm-diameter STO in CoNi film. (a) Full micromagnetic simulation and (b) macrospin model. Material parameters are identical in the simulations and similar to STOs studied in [20]. The threshold and cutoff currents and the oscillation frequencies for all harmonics are quite well approximated by the single-domain model. The curves are somewhat different in the third dimension, as the macrospin model is not very accurate in the predicting of linewidth and also due to the numerical accuracy of the Fourier transform. The single-domain model shows more harmonics than the macrospin model.**

The current-dependent frequency spectra were generated from 100 independent simulation runs, each simulation run using a different current value from 0 to 10 mA. The time-dependent magnetization dynamics was then Fourier-transformed. In experiments, such spectra are often measured by spectrum analyzers. Plotting the data this way allows comparison of simulation results from different models and comparing computational and experimental results [17].

The simulations show that for contact diameters between 30 and 50 nm, the macrospin model is a close approximation. This means that the $f(i)$ current–frequency relation of oscillation peaks, the precession modes, the threshold current for the onset of oscillations, and the cutoff current (the current when the STO layer switches to a stationary state and stops oscillating) agree well between the two models. The full micromagnetic model predicts higher oscillation bandwidth, due to nonuniformities appearing in $\mathbf{M}(\mathbf{r}, t)$. For nanomagnet diameters above 50 nm, the free layer magnetization breaks up into multiple domains during oscillation, and the linewidths, threshold, and cutoff currents predicted by the macrospin model became highly inaccurate. This means that typically for $d < 50$-nm-diameter STOs, there is a possibility to develop lumped, ODE-based models [32].

As a case study, we investigate a model of electrically coupled STOs. The magnetization oscillations modulate the STO resistance and the oscillation signal can be picked up and superposed to the driving current of each individual STO. A circuit schematic is shown in Fig. 15—this is an implementation of the star-architecture interconnection. This circuit can be straightforwardly modeled in the single-domain approximation, and details about the model are given in [20].

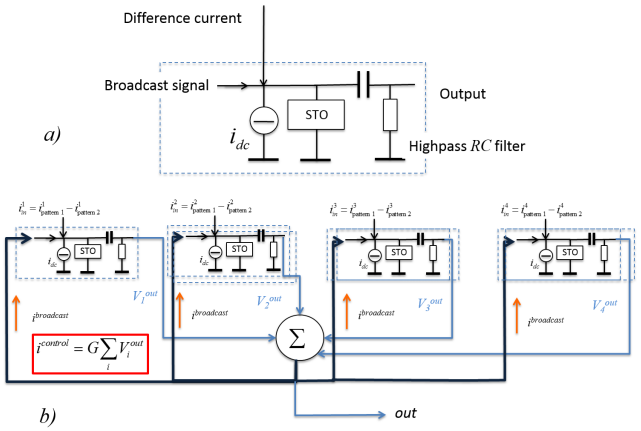


**FIGURE 15.** **Realization of the FSK scheme of Fig. 2 with STOs. (a) In the associative array, each STO is biased by a constant current, its inputs is proportional to the difference between the $\xi$ vectors and the output of the STOs connect to the broadcast amplifier via a high-pass filter. (b) Circuit schematic showing the interconnection of four STOs in the broadcast scheme (star architecture). The boxed equation shows the characteristics of the transconductance amplifier that sums STO outputs, amplifies, and broadcasts the sum signal that couples the STOs. The transconductance $G$ sets the coupling strength.**

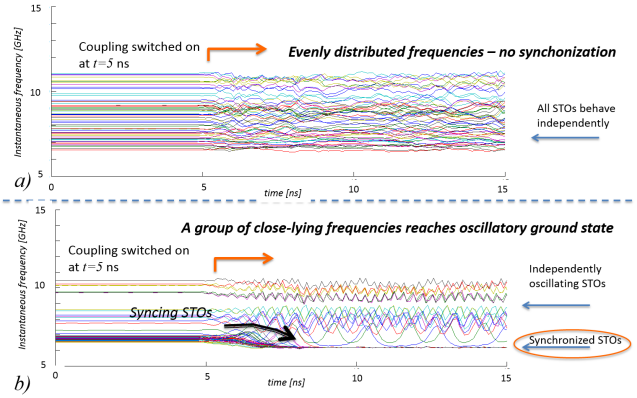


**FIGURE 16.** **Oscillator frequencies are plotted as a function of time for 64 electrically interconnected STOs. (a) Oscillator frequencies are lying too far apart to synchronize. (b) Group of STOs frequency locking.**

The coupling strength of the STOs is determined by the giant-magnetoresistance (GMR) ratio of the STOs (i.e., how strongly their resistance is changing upon oscillations) and by the transconductance of the active amplifier interconnecting them. The GMR-based STOs [17] deliver a few-ten microvolts of output voltage ($V_i^{\text{out}}$),[1] which is picked up, summed with signals from all other oscillators, and broadcasted to the input of each oscillator ($i^{\text{control}}$). The broadcasted current is typically in the order of 0.1 mA on top of few milliamps STO driving current.

According to the simulations, the phase of injection-locked STOs is not stable, while on average, the STO frequency is very close to that of the injected signal, the STO phase often undergoes jumps, before it resynchronizes with the injected signal again. Thermal agitation of the magnetic moments, which is not considered in the model, is likely another source of phase instability. This suggests that the FSK seems to be a more appropriate scheme for associative functions. Fig. 16 shows the circuit dynamics for 64 STOs interconnected using the FSK scheme. We plot the instantaneous frequency (the inverse of the time elapsed between two zero crossings of the STO signal). The coupling is abruptly switched on at $t = 5$ ns. In Fig. 16(a), the uncoupled oscillator frequencies are evenly spaced and lie too far apart to synchronize—pairwise synchronization occurs between particular frequencies, but no dominant frequency component emerges. If some oscillator frequencies form a group of like frequencies [as shown in Fig. 16(b)], then all these oscillators synchronize to a single dominant frequency component. This can be read-out and related to a DOM metric. One can clearly see that the behavior of coupled STOs differs from basic oscillator models in many respects. As shown in Fig. 16(a), even if the oscillator frequencies are far apart, oscillators interact and disturb each other's frequencies in complex ways. In many cases (unless the frequencies are very close and the coupling is strong), the array goes into a partially synchronized state, which is shown in Fig. 16(b). Some STOs are synchronized to each other, and others are periodically pulled to the synchronized group. The frequency of the synced group is not absolutely stable; it is slightly modulated by the group of unsynchronized oscillators—this is the reason why PSK would be difficult to implement.

Fig. 16(b) also shows that in this coupling scheme, STO frequencies are not independent of the degree of synchronization. A synchronized state increases the net current flow into the STOs (via the feedback) and the increasing current red-shifts (decreases) oscillation frequency.

Still, the quantification of the DOM relies on the phase-coherence of the synced STOs and their strength and stability of the dominant frequency component indicate the DOM.

## VI. CONCLUSION

We present a design of COAMA amenable to practical realization. We simulate its operation in both traditional PSK and novel FSK schemes with various models of nonlinear oscillators. The realization of these schemes with the arrays of PLL and STO is considered. The simulation shows successful recognition for the case of example matching patterns.

## ACKNOWLEDGMENT

The authors would like to thank S. Levitan, T. Roska, M. Puffal, and W. Rippard for their fruitful discussions. Other aspects of the NBAD program are covered in [33] and [34]. D. Hammerstrom is on leave from the Department of Electrical Engineering, Portland State University, Portland, OR, USA.

[1] GMR-based STO devices are all-metallic structures, where most of the net device resistance (typically a few ohms) comes from contact resistances. Overall, they are driven by a few milliamperes of current, and have a few ohms of resistance and a net magnetoresistance ratio of a few percent.

## REFERENCES


[1] G. E. Moore, "Cramming more components onto integrated circuits," *Electronics*, vol. 38, no. 8, pp. 114–117, Apr. 1965.

[2] (2011). *International Technology Roadmap for Semiconductors (ITRS)*. [Online]. Available: http://www.itrs.net

[3] S. Haykin, *Neural Networks: A Comprehensive Foundation*, 2nd ed. Englewood Cliffs, NJ, USA: Prentice-Hall, 1999.

[4] C. Mead, "Neuromorphic electronic systems," *Proc. IEEE*, vol. 78, no. 10, pp. 1629–1636, Oct. 1990.

[5] D. W. Patterson, *Artificial Neural Networks: Theory and Applications*. Englewood Cliffs, NJ, USA: Prentice-Hall, 1998.

[6] L. O. Chua and T. Roska, *Cellular Neural Networks and Visual Computing: Foundations and Applications*. Cambridge, U.K.: Cambridge Univ. Press, 2002.

[7] D. Wang and D. Terman, "Locally excitatory globally inhibitory oscillator networks," *IEEE Trans. Neural Netw.*, vol. 6, no. 1, pp. 283–286, Jan. 1995.

[8] F. C. Hoppensteadt and E. M. Izhikevich, "Oscillatory neurocomputers with dynamic connectivity," *Phys. Rev. Lett.*, vol. 82, pp. 2983–2986, Apr. 1999.

[9] M. Itoh and L. O. Chua, "Star cellular neural networks for associative and dynamic memories," *Int. J. Bifurcation Chaos*, vol. 14, no. 5, pp. 1725–1772, May 2004.

[10] F. Corinto, M. Bonnin, and M. Gilli, "Weakly connected oscillatory network models for associative and dynamic memories," *Int. J. Bifurcation Chaos*, vol. 17, no. 12, pp. 4365–4379, Dec. 2007.

[11] H. Araki, Ed., *International Symposium on Mathematical Problems in Theoretical Physics* (Lecture Notes in Physics), vol. 39. New York, NY, USA: Springer-Verlag, 1975, pp. 420–422.

[12] J. A. Acebrón, L. L. Bonilla, C. J. P. Vicente, F. Ritort, and R. Spigler, "The Kuramoto model: A simple paradigm for synchronization phenomena," *Rev. Mod. Phys.*, vol. 77, pp. 137–185, Apr. 2005.

[13] F. C. Hoppensteadt and E. M. Izhikevich, "Pattern recognition via synchronization in phase-locked loop neural networks," *IEEE Trans. Neural Netw.*, vol. 11, no. 3, pp. 734–738, May 2000.

[14] F. Macià, A. D. Kent, and F. C. Hoppensteadt, "Spin-wave interference patterns created by spin-torque nano-oscillators for memory and computation," *Nanotechnology*, vol. 22, no. 9, p. 095301, Jan. 2011.

[15] J. C. Slonczewski, "Current-driven excitation of magnetic multilayers," *J. Magn. Magn. Mater.*, vol. 159, nos. 1–2, pp. L1–L7, Jun. 1996.

[16] G. Bertotti, C. Serpico, I. D. Mayergoyz, A. Magni, M. d'Aquino, and R. Bonin, "Magnetization switching and microwave oscillations in nanomagnets driven by spin-polarized currents," *Phys. Rev. Lett.*, vol. 94, p. 127206, Apr. 2005.

[17] S. E. Russek, W. H. Rippard, T. Cecil, and R. Heindl, "Spin-transfer nano-oscillator," in *Handbook of Nanophysics: Functional Nanomaterials*, K. D. Sattler, Ed. Boca Raton, FL, USA: CRC Press, 2010.

[18] A. Slavin, "Microwave sources: Spin-torque oscillators get in phase," *Nature Nanotechnol.*, vol. 4, no. 8, pp. 479–480, Aug. 2009.

[19] W. H. Rippard, M. R. Pufall, S. Kaka, T. J. Silva, S. E. Russek, and J. A. Katine, "Injection locking and phase control of spin transfer nano-oscillators," *Phys. Rev. Lett.*, vol. 95, no. 6, pp. 067203-1–067203-4, Aug. 2005.

[20] W. H. Rippard *et al.*, "Spin-transfer dynamics in spin valves with out-of-plane magnetized CoNi free layers," *Phys. Rev. B*, vol. 81, p. 014426, Jan. 2010.

[21] P. A. Grünberg, "Nobel lecture: From spin waves to giant magnetoresistance and beyond," *Rev. Mod. Phys.*, vol. 80, pp. 1531–1540, Dec. 2008.

[22] L. Berger, "Emission of spin waves by a magnetic multilayer traversed by a current," *Phys. Rev. B*, vol. 54, pp. 9353–9358, Oct. 1996.

[23] M. Madami *et al.*, "Direct observation of a propagating spin wave induced by spin-transfer torque," *Nature Nanotechnol.*, vol. 6, no. 10, pp. 635–638, Aug. 2011.

[24] S. Kaka, M. R. Pufall, W. H. Rippard, T. J. Silva, S. E. Russek, and J. A. Katine, "Mutual phase-locking of microwave spin torque nano-oscillators," *Nature*, vol. 437, pp. 389–392, Sep. 2005.

[25] M. J. Donahue and D. G. Porter, "OOMMF user's guide, version 1.0," Nat. Inst. Standards Technol., Gaithersburg, MD, USA, Tech. Rep. NISTIR 6376, Sep. 1999. [Online]. Available: http://math.nist.gov/oommf/

[26] G. Bertotti, I. D. Mayergoyz, and C. Serpico, *Nonlinear Magnetization Dynamics in Nanosystems*. Amsterdam, The Netherlands: Elsevier, 2009.

[27] V. S. Pribiag *et al.*, "Magnetic vortex oscillator driven by d.c. spin-polarized current," *Nature Phys.*, vol. 3, pp. 498–503, May 2007.

[28] E. M. Izhikevich, *Dynamical Systems in Neuroscience: The Geometry of Excitability and Bursting*. Cambridge, MA, USA: MIT Press, 2007.

[29] A. Pikovsky, M. Rosenblum, and J. Kurths, *Synchronization: A Universal Concept in Nonlinear Sciences*. Cambridge, U.K.: Cambridge Univ. Press, 2001.

[30] F. Corinto, M. Gilli, and T. Roska, "On full-connectivity properties of locally connected oscillatory networks," *IEEE Trans. Circuits Syst. I, Reg. Papers*, vol. 58, no. 5, pp. 1063–1075, May 2011.

[31] W. F. Egan, *Phase-Lock Basics*. New York, NY, USA: Wiley, 1998.

[32] G. Csaba, A. Imre, G. H. Bernstein, W. Porod, and V. Metlushko, "Nanocomputing by field-coupled nanomagnets," *IEEE Trans. Nanotechnol.*, vol. 1, no. 4, pp. 209–213, Dec. 2002.

[33] M. R. Pufall, W. H. Rippard, G. Csaba, D. E. Nikonov, G. I. Bourianoff, and W. Porod, "Physical implementation of coherently coupled oscillator networks," *IEEE J. Exploratory Solid-State Comput. Devices Circuits*, vol. 1, pp. 76–84, Dec. 2015.

[34] Y. Fang, C. N. Gnegy, T. Shibata, D. Dash, D. M. Chiarulli, and S. P. Levitan, "Non-Boolean associative processing: Circuits, system architecture, and algorithms," *IEEE J. Exploratory Solid-State Comput. Devices Circuits*, to be published.



**DMITRI E. NIKONOV** (M'99–SM'06) received the M.S. degree in aeromechanical engineering from the Moscow Institute of Physics and Technology, Moscow, Russia, in 1992, and the Ph.D. degree in physics from Texas A&M University, College Station, TX, USA, in 1996.

He joined Intel, Santa Clara, CA, USA, in 1998. He is currently a Principal Engineer with the Components Research Group, Hillsboro, OR, USA, doing simulation and benchmarking of beyond-CMOS logic devices, and managing research programs with universities on nanotechnology.

**GYORGY CSABA,** photograph and biography not available at the time of publication.

**WOLFGANG POROD,** photograph and biography not available at the time of publication.

**TADASHI SHIBATA,** photograph and biography not available at the time of publication.

**DANNY VOILS,** photograph and biography not available at the time of publication.

**DAN HAMMERSTROM,** photograph and biography not available at the time of publication.

**IAN A. YOUNG** (M'78–SM'96–F'99) received the B.E.E. and M.Eng.Sci. degrees from the University of Melbourne, Melbourne, VIC, Australia, and the Ph.D. degree in electrical engineering from the University of California at Berkeley, Berkeley, CA, USA.

He is currently a Senior Fellow and the Director of the Exploratory Integrated Circuits with the Technology and Manufacturing Group, Intel Corporation, Hillsboro, OR, USA. He leads a research group exploring the future options for the integrated circuit in the beyond CMOS era.

**GEORGE I. BOURIANOFF,** photograph and biography not available at the time of publication.